International Telecommunication Union

ITU-R

Radiocommunication Sector of ITU

Report ITU-R RA.2512-0
(10/2022)

Technical and operational characteristics of broadband, background-limited detectors operating in the millimetre-wave regime

RA Series

Radio astronomy

International Telecommunication Union

Foreword

The role of the Radiocommunication Sector is to ensure the rational, equitable, efficient and economical use of the radio-frequency spectrum by all radiocommunication services, including satellite services, and carry out studies without limit of frequency range on the basis of which Recommendations are adopted.

The regulatory and policy functions of the Radiocommunication Sector are performed by World and Regional Radiocommunication Conferences and Radiocommunication Assemblies supported by Study Groups.

Policy on Intellectual Property Right (IPR)

ITU-R policy on IPR is described in the Common Patent Policy for ITU-T/ITU-R/ISO/IEC referenced in Resolution ITU-R 1. Forms to be used for the submission of patent statements and licensing declarations by patent holders are available from http://www.itu.int/ITU-R/go/patents/en where the Guidelines for Implementation of the Common Patent Policy for ITU-T/ITU-R/ISO/IEC and the ITU-R patent information database can also be found.

Series of ITU-R Reports

(Also available online at http://www.itu.int/publ/R-REP/en)

Series	Title
BO	Satellite delivery
BR	Recording for production, archival and play-out; film for television
BS	Broadcasting service (sound)
BT	Broadcasting service (television)
F	Fixed service
M	Mobile, radiodetermination, amateur and related satellite services
P	Radiowave propagation
RA	**Radio astronomy**
RS	Remote sensing systems
S	Fixed-satellite service
SA	Space applications and meteorology
SF	Frequency sharing and coordination between fixed-satellite and fixed service systems
SM	Spectrum management

***Note**: This ITU-R Report was approved in English by the Study Group under the procedure detailed in Resolution ITU-R 1.*

Electronic Publication
Geneva, 2022

REPORT ITU-R RA.2512-0

Technical and operational characteristics of broadband, background-limited detectors operating in the millimetre-wave regime

(Questions ITU-R 226-2/7 and ITU-R 257/7)

(2022)

1 Introduction

The cosmic microwave background (CMB) is a pervasive cold glow across the entire sky at microwave through millimetre-wave frequencies. Studying this cosmic signal informs our understanding of the Universe and has motivated the development of extremely sensitive millimetre-wave bolometric detectors and others with similar characteristics, with large fractional bandwidths of order 30% or more. Here, these detectors are referred to as background-limited because when cooled to sub-Kelvin temperatures, they achieve sensitivities that are limited only by the Earth's atmosphere. These detectors are placed on telescopes at the best millimetre observing sites on Earth, which have exceptionally low atmospheric loss. Cosmological surveys with background-limited detectors at these sites normally require years of integration time to achieve their measurement goals.

The CMB is now understood to be the relic radiation of the hot big bang associated with the origins of the observable universe, cooled through its subsequent expansion. The Nobel-prize winning discovery of the CMB in 1965 [1], was achieved through careful analysis of excess sky noise observed with a single microwave receiver at a single frequency, carefully analysed to eliminate both natural and artificial foreground radiation. Since then, the field has advanced dramatically, from first tracing out the near-perfect Planck spectrum corresponding to blackbody radiation at a thermodynamic temperature of 2.7 K [2], [3], to mapping the angular structure of the tiny variations in temperature across the sky to reveal structure in remarkable agreement with cosmological theory [4] to [8].

Observations with small telescopes onboard satellites and stratospheric balloons have been key for these observations at few-arcminute to few degree angular scales. Further progress in the field now requires observing fainter signals with better instrumental sensitivity and angular resolution, requiring large telescopes (6-metre class) which are difficult to deploy in space or on balloons. Hence, multiple ground-based telescopes are required, with broadband bolometers operating at background-limited sensitivities limited only by noise from atmospheric emission. To reach nano-Kelvin sensitivity levels, these telescopes are equipped with tens of thousands of broad-band bolometric detectors, observing patches of sky at millimetre to centimetre wavelengths for several-year surveys [9], [10]. Cosmological observations provide steadily increasing insight into the astrophysics of the early universe, and test fundamental physical theory at energy scales inaccessible to high-energy physics experiments on Earth. While all observations are generally compatible with the same overall cosmological model, this model requires the Universe to be filled with matter and energy of unknown forms, dubbed dark matter and dark energy, amounting to 95% of the total density [11]. It is also believed that when the Universe was just a fraction of a second old, it underwent a period of ultra-rapid expansion, called cosmic inflation, driven by physical processes yet poorly understood, during which in about 10^{-32} seconds the size of the Universe was multiplied by a factor of at least 10^{26} [12]. Modern CMB observations are key to confirming this hypothesis, and provide essential information about the nature of dark matter and dark energy.

Because these cosmological surveys must repeatedly survey the sky each day and night for years to gain the requisite sensitivity, CMB observations are also creating a new window on the time-varying universe. With wide bandwidth and large sky coverage, these surveys are capturing rare, faint, or short-lived events that have previously gone unnoticed. Advances in instantaneous sensitivity enabled

by increasing detector counts and wider fields of view are further opening the discovery space to investigate transient and time-variable phenomena.

Recommendation ITU-R RA.769 considers "...that radio astronomers have made useful astronomical observations from the Earth's surface in all available atmospheric windows ranging from 2 MHz to 1 000 GHz and above..." and indeed, the achievements of modern CMB experiments would not be possible but for the passive use, from remote locations, of spectrum allocated to active services. The characteristics of CMB detectors are somewhat different from the RAS observatories covered in Recommendation ITU-R RA.769 in ways that render them both more and less susceptible to terrestrial radiation [13]. On the one hand, CMB detectors typically employ large fractional bandwidths (of order 30%), use detectors carefully designed to operate at background-limited sensitivity, and accumulate years of data to integrate down to high sensitivity. The typical bandwidth of such detectors in the millimetre-wave is an order of magnitude larger than the relatively small bandwidths assumed in Recommendation ITU-R RA.769. It should also be noted that the RAS thresholds covered by Recommendation ITU-R RA.769 are calculated on the basis that a typical observing bandwidth is at most 8 GHz, which is in stark contrast to what typical bolometric detectors offer (50 GHz and more), limited by the spectral width of atmospheric windows between strong absorption features of water vapor and oxygen. On the other hand, the sidelobe suppression, scan strategies, use of multiple wave bands, and analysis techniques all needed to reject natural foregrounds in CMB experiments can help mitigate artificial foregrounds as well. Antenna sidelobes, in particular, are much more a problem for CMB measurements than they are for classical radio astronomy, as the CMB requires much higher sensitivity observations, and contributions from the side-lobe irradiation play a crucial role.

This document aims to record the geographic sites, the RAS allocations utilized for CMB experiments, instrument characteristics of the bolometric cameras used in CMB experiments, and to provide background for further study and recommendations analogous to Recommendation ITU-R RA.769.

2 Sites

The needs of CMB experiments have driven them to be located at dry, high-altitude sites with minimum atmospheric absorption and access to parts of the sky with low astrophysical foreground emission. Ground-based telescopes observing in the millimetre-wave typically observe within atmospheric windows defined by absorption from molecules including oxygen and water in the Earth's atmosphere. At exceptionally dry, high altitude sites, these atmospheric windows (shown in Fig. 2, and detailed in Table 2) have extremely low atmospheric absorption loss in typical weather.

In accordance with Recommendation ITU-R RA.769-2, these CMB experiments have been placed in geographically remote locations, which are "as free as possible from interference." This Report will assist those Administrations seeking to afford protection to these experiments, following Recommendation ITU-R RA.769-2 which states, "that administrations should afford all practicable protection to the frequencies and sites used by radio astronomers in their own and neighbouring countries and when planning global systems".

Current experiments sponsored by the United States and other administrations operate at the South Pole in the protected dark sector, and in the high Atacama Desert in northern Chile in the protected astronomical reservation under the jurisdiction of the Government of Chile. CMB experiments have also operated from Antarctic long duration balloon flights, which are not limited by atmospheric windows, and can achieve sensitivities significantly lower than described here, due to the reduced atmospheric noise at float altitudes.

The quality of these sites for millimetre-wave observations, including the magnitude of atmospheric emission noise and absorption and the resulting instrument sensitivity, is set by the precipitable water

vapor (PWV). Sites with a median (50th percentile) PWV less than 1 millimetre are extremely rare and sometimes very difficult to access (for example, Dome A in Antarctica) [14].

Locations of sites with median PWV values less than 1 mm, that have established observatories with broadband, background-limited detectors in the millimetre-wave regime are summarized in Table 1.

It should be noted that there are experiments employing broadband background-limited detectors targeting the CMB and other astrophysical observables that observe continuously from sites in addition to those described in Table 1. There are also experiments with similar characteristics that have much shorter integration times that do not observe continuously, including instruments on shared user facilities, and instruments with short-term deployments including balloon flights and other temporary platforms. Examples of these include the GroundBIRD CMB experiment at Teide Observatory in Tenerife in the Canary Islands, observations using the NIKA2 camera on the IRAM 30-metre telescope on *Pico Veleta*, Spain, as well as instruments such as e.g. ArTéMiS and CONCERTO on the 12-metre APEX telescope, located in *Parque Astronómico de Atacama*.

TABLE 1

Location of established sites for background-limited millimetre-wave CMB surveys

Site	Latitude (degree N)	Longitude (degree E)	Altitude (m)	50th percentile Precipitable Water Vapor (PWV) (mm H_2O)	5th percentile PWV (mm H_2O)
South Pole Dark Sector	−90.0	0.0	2 835	0.4	0.15
Parque Astronómico de Atacama, Chile	−23.0	−67.8	5 200	0.9	0.2

3 Key scientific observables in measurement bands

Ground-based instruments passively utilize broad frequency bands which are designed to fit within atmospheric transmission windows near the CMB peak frequency. The bandwidths are as wide as possible to maximize sensitivity in these photon-noise dominated instruments. Since the noise in these instruments is dominated by atmospheric noise, their sensitivity is limited by atmospheric conditions. Typical values for atmospheric loading and noise across these atmospheric windows is detailed in Table 2, for atmospheric properties for the sites listed in Table 1.

The CMB has a thermal blackbody emission spectrum peaking at 160 GHz. By surveying the sky at several different frequencies, the CMB component can be isolated from other sources of foreground emission with different spectral signatures, including Galactic synchrotron and dust emission, and the Sunyaev-Zeldovich effect, which is a distortion of the CMB blackbody by galaxy clusters that causes a frequency-dependent change in intensity. The relevant measurement band for these scientific observables is listed in Table 2.

FIGURE 1

The faint CMB polarization frequency spectrum is shown along with other bright astrophysical components. The measurement bands for the Planck satellite are shown as grey vertical bands. Figure from Planck Collaboration IV 2018 [15]

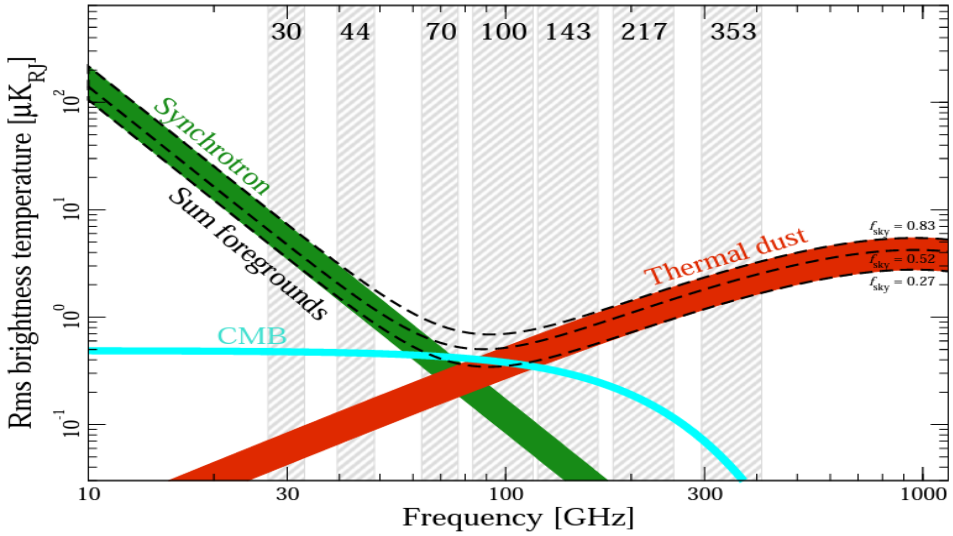

FIGURE 2

The brightness temperature is shown for typical weather conditions for the sites in Table 1, as well as in contrast, a typical high elevation mid-latitude site on Earth. Atmospheric information calculated using [16]

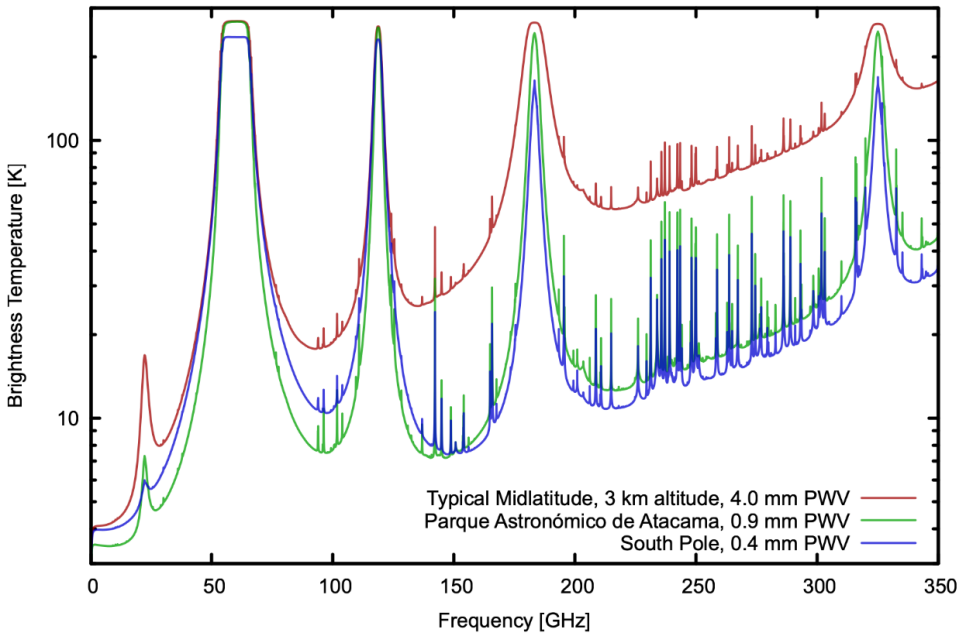

TABLE 2

Measurement bands and key observables

Measurement band (1)	**RAS allocations and identifications**	**Scientific observable**	**Typical band-integrated atmospheric power (pW)** (2)	**Typical atmospheric noise equivalent power (aW $Hz^{-1/2}$)** (2)
21.5-30 GHz	22.01-22.21 GHz, 23.07-23.12 GHz (**5.149**) 23.6-24 GHz (Primary **5.340**)	Galactic synchrotron; CMB blackbody	0.6	10
30-47.5 GHz	31.2-31.3 GHz (**5.149**) 31.3-31.8 GHz (Primary **5.340**, **5.534A**) 36.43-36.5 GHz (**5.149**) 42.5-43.5 GHz (Primary **5.149**, **5.551H**, **5.551I**)	CMB blackbody; Galactic synchrotron	2.6	30
72-118 GHz	76-77.5 GHz (Primary **5.149**) 77.5-79 GHz (Secondary **5.149**) 79-86 GHz (Primary **5.149**) 86-92 GHz (Primary **5.340**) 92-94 GHz (Primary **5.149**) 94-94.1 GHz (Secondary **5.562A**) 94.1-100 GHz (Primary **5.149**) 100-102 GHz (Primary **5.340**) 102-105 GHz (Primary **5.149**) 105-109.5 GHz (Primary **5.149**, **5.562B**) 109.5-111.8 GHz (Primary **5.340**) 111.8-114.25 GHz (Primary **5.149**, **5.562B**) 114.25-116 GHz (Primary **5.340**)	CMB blackbody; Galactic dust emission; Galactic synchrotron; Sunyaev-Zeldovich effect	3	40
122-180 GHz	123-128.33 GHz (Secondary) 128.33-128.59 GHz, 129.23-129.49 GHz (Secondary **5.149**) 129.49-130 GHz (Secondary) 130-134 GHz (Primary **5.149**, **5.562S**) 134-136 GHz (Secondary) 136-148.5 GHz (Primary **5.149**) 148.5-151.5 GHz (Primary **5.340**) 151.5-158.5 GHz (Primary **5.149**) 164-167 GHz (Primary **5.340**) 168.59-168.93 (**5.149**) 171.11-171.45 GHz (**5.149**) 172.31-172.65 GHz (**5.149**) 173.52-173.85 GHz (**5.149**)	CMB blackbody; Galactic dust emission; Galactic synchrotron; Sunyaev-Zeldovich effect	6	50

TABLE 2 (*end*)

Measurement band [1]	**RAS allocations and identifications**	**Scientific observable**	**Typical band-integrated atmospheric power (pW)** [2]	**Typical atmospheric noise equivalent power (aW Hz$^{-1/2}$)** [2]
200-256 GHz	200-209 GHz (Primary **5.340**) 209-226 GHz (Primary **5.149**) 226-231.5 GHz (Primary **5.340**) 241-250 GHz (Primary **5.149**) 250-252 GHz (Primary **5.340**) 252-275 GHz (Primary **5.149**)	CMB blackbody; Galactic dust emission; Sunyaev-Zeldovich effect	13	100
256-315 GHz	252-275 GHz (Primary **5.149**) 275-323 GHz (**5.565**)	CMB blackbody; Galactic dust emission; Sunyaev-Zeldovich effect	16	120

(1) Band edges are estimates of where band drops to ~10% of its peak value. It should be noted that the CMB measurement bands are wider than the specific allocations to RAS in Article **5** of the RR. The RAS allocations and identifications are noted in column 2.

(2) aW: attowatt, the SI unit of power equal to 10^{-18} Watts. Noise equivalent power (NEP) is defined as the total power in the measurement band that can be detected with a signal to noise ratio of 1 with one second of integration, corresponding to a post-detection bandwidth of 1 Hz. NEP scales as the square root of post-detection bandwidth. Atmospheric NEP and atmospheric power figures assume an elevation of 50 degrees above the horizon and precipitable water vapor (PWV) of 0.5 mm. Note that the unusually low surface-level PWV assumed here is characteristic of CMB observing sites (as detailed in Table 1).

4 Instruments

Relevant observatories, observing bands, and detector characteristics are summarized in Tables 3 and 4. Instruments utilize the frequency bands described in Table 2. CMB instruments are typically designed to measure polarized emission, both in order to study the polarization of the CMB, and to isolate and remove unpolarized atmospheric emission.

Aspects of CMB instrument design that enable their excellent sensitivity also render them vulnerable to radio-frequency interference across a wide range of frequencies. Bolometers are inherently broadband and sensitive to all incident power, and frequency bands are defined by a combination of on-chip microwave filters at the antenna, and reflective and absorptive filters within the optical path. High transmissivity within band must be maintained while rejecting out-of-band frequencies. The detection band definition is dominated by the on-chip filters integrated into the cryogenic bolometer arrays. Fabrication technology limits the accuracy of band centres and fractional bandwidths of these filters on the order of a few percent.

Another emerging technique for background-limited detectors is kinetic inductance detectors, which are superconducting resonators that use Cooper pairs to detect incoming radiation. Its effect on the resonator is transferred to a RF readout system, which can measure the responses of hundreds of pixels in a single RF line. The NIKA2 instrument installed within the IRAM telescope located on Mount *Pico Veleta*, Spain is one of the very first to be equipped with KID technology for use in millimetric astronomy.

Both types of highly sensitive low temperature detectors are basically thermometers: they simply measure all input radiation in a given band. Because of this, RFI mitigation is usually not possible, except for removing affected samples completely, which can lead to a large fractional loss of observing time.

Many instruments have a large aperture to the sky that is heavily filtered against transmission of higher frequencies (which would cause thermal loading at the sub-Kelvin focal plane) but largely unshielded against lower frequencies, because such shielding would have negative impacts on in-band transmissivity and sensitivity. These unshielded apertures can range in diameter from ~1 cm to ~1 m, depending on instrument design, and are an important variable in assessing complex coupling mechanisms to out-of-band emission. Other potential sources of coupling include long runs of wiring and weakly coupled ground planes, which can be necessary when balancing cryogenic temperature isolation with electrical performance.

These instruments are designed to be as well shielded from stray radiation as possible, while maintaining a large field of view on the sky. Minimizing antenna sidelobes is an important design consideration, as well as characterizing unavoidable sidelobes and terminating them on an absorbing surface or the cold sky. Effective co-moving shielding can be more difficult for larger aperture telescopes. Even with sidelobe suppression, coupling to sidelobes with brighter sources including the Sun and artificial sources can result in significant contamination.

TABLE 3

Instruments at *Parque Astronómico de Atacama*, Chile

Telescope or project name	Instrument, years of operation, detector count	Band centre (GHz)	Fractional bandwidth	Antenna beamwidth (degree)	Directivity gain (dBi)	Instrument field of view (degree)	Primary aperture (m)	Unshielded aperture (m)
Atacama Cosmology Telescope [17],[18],[19]	Millimeter Bolometric Array Camera 2007-2010 3 072 detectors	149 220 277	0.12 0.077 0.075	0.023 0.017 0.015	78 80 81	1	6	0.21
	ACTPol 2013-2016 3 068 detectors	98 147 150	0.39 0.28 0.34	0.034 0.025 0.022	74 77 78	1	6	0.34 0.34 0.64
	Advanced ACTPol 2016-present 5 736 detectors	27 38 96 149 228	0.23 0.4 0.3 0.28 0.28	0.11 0.08 0.034 0.023 0.017	64 67 74 77 80	1	6	0.34 0.34 0.66 0.66 0.32
Atacama B-Mode Search [20]	ABS 2012-2014 480 detectors	145	0.25	0.53	51	22	0.25	0.3
Cosmology large angular scale surveyor [21]	Q-band receiver 2016-present 72 detectors	38	0.32	1.58	32	19.6	0.6	0.35
	W-band receiver 2018-present 1 036 detectors	93	0.34	0.62	40	24.4	0.6	0.35
	G-band dichroic receiver 2019-present 1 020 detectors	147 216	0.21 0.17	0.38 0.27	44 47	18.9	0.6	0.35

TABLE 3 (*end*)

Telescope or project name	Instrument, years of operation, detector count	Band centre (GHz)	Fractional bandwidth	Antenna beamwidth (degree)	Directivity gain (dBi)	Instrument field of view (degree)	Primary aperture (m)	Unshielded aperture (m)
POLARBEAR Simons Array [22],[23],[24]	POLARBEAR-1 2012-2017 1 274 detectors	148	0.26	0.06	69	2.8	2.5	0.3
	POLARBEAR-2 2018 – current 22 764 detectors	89.5 148 227 275	0.324 0.26 0.2 0.15	0.09 0.06 0.05 0.04	65 69 70 72	4.8	2.5	0.5

TABLE 4

Instruments at South Pole Dark Sector

Telescope or project name	Instrument, years of operation detector count	Band centre (GHz)	Fractional bandwidth	Antenna beamwidth (degree)	Directivity gain (dBi)	Instrument field of view (degree)	Primary aperture (m)	Unshielded aperture (m)
BICEP/Keck [25],[26]	BICEP1 2006-2008 98 detectors	95 150 220	0.23 0.26 0.30	0.93 0.6 0.42	45 49 52	18	0.25	0.25
	BICEP2 2010-2012 512 detectors	150	0.26	0.5	50	15	0.26	0.26
	Keck Array 2012-2019 1 824 detectors	95 150 220 270	0.23 0.26 0.24 0.18	0.72 0.5 0.35 0.28	47 50 53 56	15	0.26	0.26

TABLE 4 (*end*)

Telescope or project name	Instrument, years of operation detector count	Band centre (GHz)	Fractional bandwidth	Antenna beamwidth (degree)	Directivity gain (dBi)	Instrument field of view (degree)	Primary aperture (m)	Unshielded aperture (m)
	BICEP3 2015-current 2 560 detectors	95	0.23	0.4	52	27.4	0.52	0.52
	BICEP Array 2020-current 32 724 detectors	30 40 95 150 220 270	0.27 0.25 0.23 0.26 0.24 0.18	1.27 0.95 0.4 0.25 0.18 0.15	42 45 52 56 59 61	28	0.52	0.52
South Pole Telescope [27],[28],[29]	SPT-SZ 2017-2011 860 detectors	97.6 152.9 218.1	0.321 0.242 0.225	0.028 3 0.02 0.016 7	75. 78 80	1	10	0.35
	SPTPol 2012-2016 1 536 detectors	94.1 148.5	0.402 0.306	0.028 3 0.02	75 78	1.2	10	0.35
	SPT-3G 2016-current 16 260 detectors	94 147 220	0.281 0.221 0.244	0.026 2 0.019 5 0.017 3	76 78 79	1.9	10	0.685

References

[1] A. A. Penzias and R. W. Wilson, The Astrophysical Journal, vol. 142, pp. 419-421 (1965)

[2] J. C. Mather *et al.*, The Astrophysical Journal, vol. 420, p. 439 (1994)

[3] D. J. Fixsen *et al.*, The Astrophysical Journal, vol. 473, p. 576 (1996)

[4] G. F. Smoot *et al.*, The Astrophysical Journal Letters, vol. 396, p. L1 (1992)

[5] P. de Bernardis *et al.*, Nature, Volume 404, Issue 6781, pp. 955-959 (2000)

[6] S. Hanany *et al.*, The Astrophysical Journal, vol. 545, Issue 1, pp. L5-L9 (2000)

[7] C. L. Bennett *et al.*, The Astrophysical Journal Supplement Series, vol. 148, Issue 1, pp. 1-27 (2003)

[8] Planck Collaboration, Astronomy & Astrophysics, Volume 571, id.A1, 48 pp. (2014)

[9] Peter Ade *et al.*, Journal of Cosmology and Astroparticle Physics, Issue 02, article id. 056 (2019)

[10] K. N. Abazajian *et al.*, arXiv e-prints, arXiv:1610.02743

[11] Kenath Arun *et al.*, Advances in Space Research, Vol. 60, Issue 1, pp. 166-186 (2017)

[12] J. Martin, arXiv e-prints, arXiv:1502.05733

[13] D. R. Barron *et al.*, Proc. SPIE 12190-1 (July 2022), arXiv pre-print: arXiv:2207.13204

[14] C. L. Kuo, The Astrophysical Journal, Volume 848, Issue 64 (2017)

[15] Planck Collaboration, A&A 641, A4 (2020)

[16] S. Paine. (2022) The am atmospheric model (12.2). Zenodo. https://doi.org/10.5281/zenodo.6774376

[17] R. J. Thornton *et al.*, The Astrophysical Journal Supplement Series, Vol. 227, Issue 2 (2016)

[18] D. S. Swetz *et al.*, The Astrophysical Journal Supplement Series, Vol. 194, Issue 2 (2011)

[19] Sigurd Naess *et al.*, Journal of Cosmology and Astroparticle Physics, Volume 2020, Issue 12, p. 046 (2020).

[20] Akito Kusaka *et al.*, Journal of Cosmology and Astroparticle Physics, Volume 2018, Issue 9, p. 005 (2018)

[21] Sumit Dahal *et al.*, The Astrophysical Journal, Volume 926, Issue 1, p. 33 (2022)

[22] Z. Kermish *et al.*, Proc. SPIE, Volume 8452, 84521C (2012)

[23] A. Suzuki et al., Journal of Low Temperature Physics, Vol. 184, pp. 805-810 (2016)

[24] B. Westbrook *et al.*, Journal of Low Temperature Physics, Vol. 193, pp. 758-770 (2018)

[25] Y. D. Takahashi *et al.*, The Astrophysical Journal, Vol. 711, pp. 1141-1156 (2010)

[26] L. Moncelsi *et al.*, Proc. SPIE, Vol. 11453, 1145314 (2020)

[27] J. E. Carlstrom *et al.*, Publications of the Astronomical Society of the Pacific, Vol. 123, Issue 903, pp. 568 (2011).

[28] J. E. Austermann *et al.*, Proc. SPIE, Vol. 8452, id. 84521E (2012)

[29] J. A. Sobrin *et al.*, The Astrophysical Journal Supplement Series, Vol. 258, Issue 2 (2022)